Analytical investigation on mean and turbulent velocity fields of a plane jet*

Mi Jian-Chun(米建春)† and Feng Bao-Ping(冯宝平)

Department of Energy & Resources Engineering, College of Engineering, Peking University, Beijing 100871, *China*

(Received 28 December 2010; revised manuscript received 20 February 2011)

This paper analyses the downstream developments of the mean and the turbulent velocity fields of a plane jet. Based on the conservation of mass and the conservation of momentum, the mean-velocity half width (reflecting the jet spread rate) and the relative mass flow rate (jet entrainment) are related to the decay rate of the centreline mean velocity. These relations are not subject to self-preservation. Both analytical and experimental results suggest that the jet spread rate (K_1) and the entrainment rate (K_3) (and thus the decay rate K_2) can be well estimated from the centreline velocity, i.e., $K_1 \approx 0.6K_2$ and $K_3 \propto K_2$. The effect of initial mean velocity and RMS velocity profiles on the downstream mean velocity field appears to be embodied in the constants K_1 K_2 and K_3. The analytical relationship for the self-preserving Reynolds shear stress, obtained for the first time, works well.

Keywords: turbulent plane jet, momentum conservation, Reynolds shear stress

PACS: 47.27.–i, 47.27.wg **DOI:** 10.1088/1674-1056/20/7/074701

1. Introduction

This study is to analytically investigate the turbulent flow-field characteristics of isothermal plane jets. Such jet flows have received significant attention because of their simplicity in configuration and their fundamental significance as a basic flow for the turbulence research.

The initial conditions of a plane jet are conventionally defined to be the exit Reynolds number $R_e(\equiv U_b H/\gamma$ with U_b being the momentum-averaged exit mean velocity, H being the nozzle height and γ being the kinematic viscosity), the lateral exit profiles of the mean velocity and the turbulence intensity, the aspect ratio A_r ($\equiv w/H$ with w being the long nozzle width of the plane nozzle), the nozzle-exit geometric profiles and the global density ratio of the jet fluid to the ambient fluid. The downstream development of the jet also depends on the boundary conditions, e.g., the presence or the absence of side walls for the plane jet.

It has been widely accepted[1−22] that a jet issuing into quiescent surroundings continuously re-adjusts its dynamical behaviour relative to its initial state, so that it asymptotically attains a self-similar state in the far field. Previously this asymptotic state was expected to depend only on the rate of momentum addition and to be independent of other initial conditions.[23] That is the asymptotic growth rates of all jets are universal and the asymptotic normalised mass flow rates of all jets are identical, regardless of any differences in jet initial conditions except for the momentum addition rate and the exit Reynolds number R_e. However, this past view has later been proved, both analytically and experimentally, to be wrong (see, e.g., Refs. [1] and [2]). Self-preserving relations for the half width and for the centreline mean velocity of a plane jet were often checked by the methods in the previous work. However, the relationship between the exit flow field and the details of the self-similar state has not been investigated so far.

The objective of the present study is first to analyse the statistical turbulent flow field of a free plane jet based on the conservation of momentum and the conservation of mass and then to verify the analytical result with previous experiment results. Specifically, we will examine the influences of the jet initial mean velocity and the RMS velocity profiles on the downstream mean velocity field, on the entrainment rate and on the Reynolds shear stress.

*Project supported by the National Natural Science Foundation of China (Grant No. 10921202).

†Corresponding author. E-mail: jcmi@coe.pku.edu.cn

© 2011 Chinese Physical Society and IOP Publishing Ltd

2. Basic analysis

2.1. General case

Here we consider a turbulent free plane jet (Fig. 1) that is statistically two-dimensional, stationary, incompressible and not subject to any external body force.

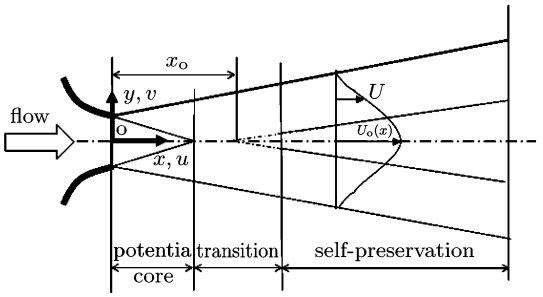


Fig. 1. Schematic view of a plane turbulent jet, with the coordinate system and key notations presented.

Applying the principles of conservation of mass and conservation of momentum to the jet passing through the control volume, we obtain an equation for the time-averaged stream-wise momentum

$$\int_{-\infty}^{\infty} \rho(\langle U\rangle^2 + \langle u^2\rangle - \langle v^2\rangle)\,\mathrm{d}y = \int_{-H/2}^{H/2} \rho_\mathrm{o}\langle U_\mathrm{o}^2\rangle\,\mathrm{d}y, \quad (1)$$

where the angular brackets denote the time averaging; the subscript 'o' refers to the nozzle exit; U and u are the stream-wise components of the instantaneous velocity and the velocity fluctuation, respectively (note: $U = \langle U\rangle + u$ and $\langle u\rangle = 0$); v is the lateral component of the velocity fluctuation; ρ_o is the density of the original jet fluid and $\rho(x)$ is the fluid density at position x, $\rho = \rho_\mathrm{o}$ for incompressibility. Using the local centreline velocities $U_\mathrm{c}(x) = \langle U\rangle(x,0)$ with $U_\mathrm{oc} = \langle U\rangle(0,0)$, the local jet half-velocity width $y_{1/2}$, at which $\langle U\rangle(x, y_{1/2}) = 0.5U_\mathrm{c}$ and H as the normalisation scales, we can rewrite Eq. (1) as

$$A_1 y_{1/2} U_\mathrm{c}^2 = B_1 H U_\mathrm{oc}^2, \quad (2)$$

where

$$A_1 = \int_{-\infty}^{\infty} (f^2 + g_{11} - g_{22})\,\mathrm{d}\eta,$$

with $f = \langle U\rangle(x,\eta)/U_\mathrm{c}$, $g_{11} = \langle u^2\rangle(x,\eta)/U_\mathrm{c}^2$, $g_{22} = \langle v^2\rangle(x,\eta)/U_\mathrm{c}^2$ and $\eta = y/y_{1/2}$; $B_1 = \int_{-1/2}^{1/2} e^2(\xi)\,\mathrm{d}\xi$ with $e(\xi) = \langle U\rangle(0,\xi)/U_\mathrm{oc}$ and $\xi = y/H$. It follows that

$$\frac{y_{1/2}}{H} = C_1 \left(\frac{U_\mathrm{oc}}{U_\mathrm{c}}\right)^2, \quad (3)$$

with $C_1 = B_1 A_1^{-1}$. The bulk mean velocity through the nozzle exit can be related with U_oc by

$$U_\mathrm{b} = H^{-1}\int_{-H/2}^{H/2} \langle U_\mathrm{o}\rangle\,(y)\,\mathrm{d}y = B_2 U_\mathrm{oc}, \quad (4)$$

where $B_2 = \int_{-1/2}^{1/2} e(\xi)\,\mathrm{d}\xi$. Therefore, Eq. (3) may be rewritten as

$$\frac{y_{1/2}}{H} = C_2 \left(\frac{U_\mathrm{b}}{U_\mathrm{c}}\right)^2 \quad (5)$$

with $C_2 = B_1 A_1^{-1} B_2^{-2}$.

From the practical point of view, one of the most important parameters of the mean jet flow is the entrainment rate, which can be measured by the ratio of the mass flow rate at x (M_x) to the initial counterpart (M_o), i.e., M_x/M_o. At the jet exit, the mean rate, at which mass is added to the jet, can be expressed as

$$M_\mathrm{o} = \rho_\mathrm{o} U_\mathrm{b} H w. \quad (6)$$

At distance x downstream from the jet exit, the mass flow rate, which increases due to the jet entrainment, becomes

$$M_x = \int_{-\infty}^{\infty} \rho\,\langle U\rangle\,(x,y) w\,\mathrm{d}y = A_2 \rho y_{1/2} w U_\mathrm{c}, \quad (7)$$

where $A_2 = \int_{-\infty}^{\infty} f(\eta)\,\mathrm{d}\eta$. It follows that the ratio M_x/M_o can be expressed as ($\rho = \rho_\mathrm{o}$)

$$\frac{M_x}{M_\mathrm{o}} = A_2 \frac{\rho}{\rho_\mathrm{o}} \frac{y_{1/2}}{H} \frac{U_\mathrm{c}}{U_\mathrm{b}}. \quad (8)$$

Substituting Eq. (3) or Eq. (5) into Eq. (8) leads to

$$\frac{M_x}{M_\mathrm{o}} = C_3 \frac{U_\mathrm{co}}{U_\mathrm{c}} \quad (9)$$

with $C_3 = (A_2 B_1)(A_1 B_2)^{-1}$, or

$$\frac{M_x}{M_\mathrm{o}} = C_4 \frac{U_\mathrm{b}}{U_\mathrm{c}} \quad (10)$$

with $C_4 = (A_2 B_1)(A_1 B_2^2)^{-1}$. Note that relations given in Eqs. (3), (5), (9) and (10) are not subject to any conditions for the self-similarity of the flow, in which f, g_{11} and g_{22} are all independent of x.

2.2. Similarity solutions

It has been long observed experimentally that for the turbulent plane jet, all the lateral profiles of the normalized mean velocity $f = \langle U\rangle/U_\mathrm{c}$ and the Reynolds stresses $g_{11} = \langle u^2\rangle(x,\eta)/U_\mathrm{c}^2$, $g_{22} = \langle v^2\rangle(x,\eta)/U_\mathrm{c}^2$ and $g_{12} = \langle uv\rangle/U_\mathrm{c}^2$ as a function of $\eta = y/y_{1/2}$ become self-similar, i.e., independent of x, as the flow proceeds sufficiently downstream into the

far field. In such a self-similar far-field region, the use of the self-similar profiles can reduce the boundary-layer equation of the axial mean momentum (neglecting the viscous term)

$$\langle U\rangle \frac{\partial \langle U\rangle}{\partial x} + \langle V\rangle \frac{\partial \langle U\rangle}{\partial y} = -\frac{\partial \langle uv\rangle}{\partial y} \tag{11}$$

to an ordinary differential equation. Using $\langle U\rangle = U_{\rm c}(x)f(\eta)$, $\langle uv\rangle = U_{\rm c}^2(x)g_{12}(\eta)$ and the continuity equation

$$\frac{\partial \langle U\rangle}{\partial x} + \frac{\partial \langle V\rangle}{\partial y} = 0,$$

we obtain

$$\begin{aligned}
&\frac{\partial \langle U\rangle}{\partial x} = \frac{{\rm d}U_{\rm c}}{{\rm d}x} f - \frac{U_{\rm c}}{y_{1/2}} \frac{{\rm d}y_{1/2}}{{\rm d}x} f'\eta,\\
&\frac{\partial \langle U\rangle}{\partial y} = \frac{U_{\rm c}}{y_{1/2}} f', \quad \frac{\partial \langle uv\rangle}{\partial y} = \frac{U_{\rm c}^2 g_{12}'}{y_{1/2}},\\
&\langle V\rangle = U_{\rm c}\frac{{\rm d}y_{1/2}}{{\rm d}x}\eta f - \left(y_{1/2}\frac{{\rm d}U_{\rm c}}{{\rm d}x} + U_{\rm c}\frac{{\rm d}y_{1/2}}{{\rm d}x}\right)\\
&\qquad \times \int_0^\eta f(\eta^*){\rm d}\eta^*,
\end{aligned}$$

where a prime denotes the differentiation with respect to η. Substituting the above terms into Eq. (11) leads to the following ordinary differential equation:

$$\left(\frac{y_{1/2}}{U_{\rm c}}\frac{{\rm d}U_{\rm c}}{{\rm d}x}\right) f^2 - \left[\frac{{\rm d}(y_{1/2}U_{\rm c})}{U_{\rm c}{\rm d}x}\right] f' \times \int_0^\eta f(\eta^*){\rm d}\eta^* = -g_{12}'. \tag{12}$$

Since the right-hand side is only a function of η, so should be the left-hand side. Hence, the terms in square brackets must be independent of x; in other words,

$$\frac{y_{1/2}}{U_{\rm c}}\frac{{\rm d}U_{\rm c}}{{\rm d}x} = \frac{K_0}{2}, \tag{13}$$

$$\frac{{\rm d}(y_{1/2}U_{\rm c})}{U_{\rm c}{\rm d}x} = \frac{y_{1/2}}{U_{\rm c}}\frac{{\rm d}U_{\rm c}}{{\rm d}x} + \frac{{\rm d}y_{1/2}}{{\rm d}x} = \frac{K_1}{2}, \tag{14}$$

where K_0 and K_1 are experimental constants, depending only on initial conditions of the jet. It is derived from Eq. (2) that

$$\frac{y_{1/2}}{U_{\rm c}}\frac{{\rm d}U_{\rm c}}{{\rm d}x} = -\frac{1}{2}\frac{{\rm d}y_{1/2}}{{\rm d}x}. \tag{15}$$

We can obtain from Eqs. (13) and (15) that $K_1 = -K_0$ and

$$\frac{y_{1/2}}{H} = K_1\frac{x-x_{\rm o}}{H}, \tag{16}$$

where $x_{\rm o}$ is the x location of the jet virtual origin and the jet is assumed to spread linearly. By substituting this linear relation into Eq. (5), we obtain

$$\left(\frac{U_{\rm b}}{U_{\rm c}}\right)^2 = K_2\frac{x-x_{\rm o}}{H}, \tag{17}$$

with $K_2 = K_1/C_2$. In addition, according to Eq. (10), the normalised mass flow rate, $M_x/M_{\rm o}$, can be expressed as

$$\begin{aligned}
\frac{M_x}{M_{\rm o}} &= C_4 K_2^{1/2}\left(\frac{x-x_{\rm o}}{H}\right)^{1/2}\\
&= \left(K_3\frac{x-x_{\rm o}}{H}\right)^{1/2},
\end{aligned} \tag{18}$$

where the constant $K_3 = C_4^2K_2$ is the slope of the linear $(M_x/M_{\rm o})^2$, which is a measure of the entrainment rate of the plane jet flow. With Eqs. (14) and (15), equation (12) can reduce to

$$f^2 + f'\int_0^\eta f(\xi){\rm d}\xi = 2K_1^{-1}g_{12}'. \tag{19}$$

As indicated in Ref. [4], in the self-similar far-field region, the lateral profile of $f = U/U_{\rm c}$ as a function of $\eta = y/y_{1/2}$ is independent of the initial velocity profiles. Thus it follows that the solution of Eq. (19) for f should not be correlated with K_1, which is possible only when $g_{12} = K_1\lambda(\eta)$ with λ independent of K_2. Previous measurements (e.g., Refs. [3] and [4]) have also consistently suggested that f can be well approximated by the following Gaussian distribution (see Fig. 5 in Section 3.2)

$$f(\eta) = \frac{\langle U\rangle}{U_{\rm c}} = {\rm e}^{-\eta^2\ln 2}. \tag{20}$$

Substitution of this distribution into Eq. (19) leads to

$$\begin{aligned}
g_{12}(\eta) &= \frac{\langle uv\rangle}{U_{\rm c}^2} = \frac{K_1}{2}\left[\sqrt{\frac{\pi}{8\ln 2}}{\rm erf}\left(\eta\sqrt{2\ln 2}\right)\right.\\
&\quad \left. - G(\eta)\sqrt{\pi\ln 2}\right],
\end{aligned} \tag{21}$$

where

$$G(\eta) = \int_0^\eta \xi\,{\rm e}^{-\xi^2\ln 2}{\rm erf}\left(\eta\sqrt{\ln 2}\right){\rm d}\xi,$$

and

$${\rm erf}(\eta) = \frac{2}{\sqrt{\pi}}\int_0^\eta {\rm e}^{-\xi^2}{\rm d}\xi$$

is the error function. The dependence of g_{12} on the initial conditions of the jet is embodied in K_1. The jet spreading rate may vary with different initial velocity profiles (see Section 3.1). Since the Reynolds shear stress

$$\langle uv\rangle = -\gamma_{\rm t}\frac{\partial \langle U\rangle}{\partial y} = -\frac{\gamma_{\rm t}U_{\rm c}}{y_{1/2}}f'$$

or

$$g_{12} = -\frac{\gamma_{\rm t}}{U_{\rm c} y_{1/2}} f'$$

with $\gamma_{\rm t}$ being the turbulent viscosity, the normalized viscosity can be expressed as

$$\gamma_{\rm t}^* = \frac{\gamma_{\rm t}}{U_{\rm c} y_{1/2}} = -\frac{K_1}{4\eta\sqrt{\ln 2}} \left[\frac{\sqrt{\pi/2}}{2\ln 2} {\rm erf}\left(\eta\sqrt{2\ln 2}\right) - \sqrt{\pi} G(\eta) \right] {\rm e}^{\eta^2 \ln 2}, \quad (22)$$

which obviously varies with K_1.

The total contributions of g_{11} and g_{22} to the constant $A_1 = \int_{-\infty}^{\infty} (f^2 + g_{11} - g_{22}) {\rm d}\eta$ are generally less than 4% (see Fig. 10 in Section 3.3), which is much smaller than that ($\approx 96\%$) of f. The contribution from f is independent of the initial conditions. Hence, the initial condition effect on A_1 and A_2 could be negligible. We therefore obtain that $A_1 \approx 1.5$ and $A_2 \approx 2.13$ based only on f for all plane jets. It follows that $C_1 \approx 0.6643 B_1 C_2 \approx 0.6643 B_1 B_2^{-2}$, $C_3 \approx 1.4142 B_1 B_2^{-1}$, and $C_4 \approx 1.4142 B_1 B_2^{-2}$.

3. Analytic and experimental results

3.1. Dependence of constants B_1, B_2, $C_1 - C_4$ on initial profiles of mean and RMS velocities

Figures 2 and 3 show previous measurements[34] of initial mean velocity $e(\xi) = \langle U \rangle / U_{\rm oc}$ and RMS velocity $h(\xi) = u'/U_{\rm oc}$ over the range $-0.5 \le y/H \le 0.5$. Although all previous mean exit velocity data individually form a quasi top-hat profile, differences between the profiles are evident due to the varying initial conditions. The Reynolds number effect is obvious on both $e(\xi)$ and $h(\xi)$. As $R_{\rm e}$ increases, the exit velocity profile becomes flatter and the horizontal region of uniformity widens.[4] It is also demonstrated in Ref. [3] that the normalised mean velocity profiles do not become identical even at $R_{\rm e} = 7000$, but become nearly identical when $R_{\rm e} \ge 10000$. The dependence of $h(\xi)$ is more obvious.

Figure 3 indicates that there are discernible differences presented in $h = u'/U_{\rm oc}$ for the jets with different $R_{\rm e}$ values. For the jet with $R_{\rm e} = 3000$,[4] h is approximately 0.42% at $\xi < 0.4$ and approaches a maximum ($\sim$6%) in the thin shear layer near the edge ($\xi > 0.4$). For the jet with $R_{\rm e} = 7000$,[4] h is even lower ($\approx 0.25\%$) both at $\xi < 0.4$ and near the edges ($\sim$4%). Hence, h contributes very little to the constant $B_1 (= \int_{-1/2}^{1/2} (e^2 + h^2) {\rm d}\xi)$; namely, $B_1 \approx \int_{-1/2}^{1/2} e^2 {\rm d}\xi$. For example, the contribution of h to the case with $R_{\rm e} = 3000$ is about 0.36% and is less than 0.2% for other cases considered.

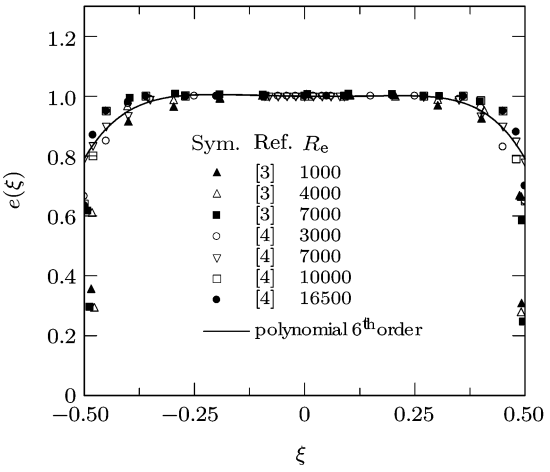


Fig. 2. Distributions of exit mean velocity.

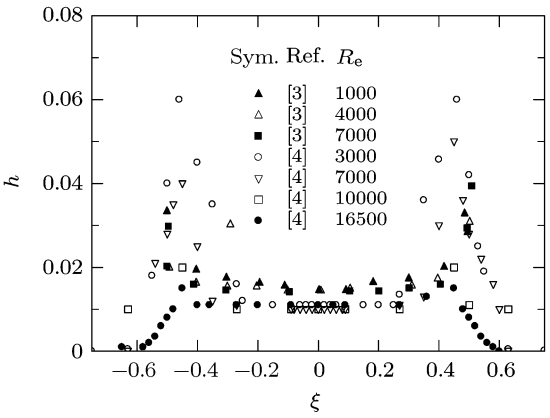


Fig. 3. Distributions of exit turbulence intensity.

Figure 4 shows the results of B_1 $(= \int_{-1/2}^{1/2} e^2 {\rm d}\xi)$ and B_2 $(= \int_{-1/2}^{1/2} e {\rm d}\xi)$, together with their related constants $C_1 \approx 0.6643 B_1 C_2 \approx 0.6643 B_1 B_2^{-2}$, $C_3 \approx 1.4142 B_1 B_2^{-1}$, and $C_4 \approx 1.4142 B_1 B_2^{-2}$. The B_1 and B_2 are calculated with the velocity profiles $e(\xi)$ from Refs. [3] and [4]. We fit the experimental data points of $e(\xi)$ by integrating the polynomial, e.g., those from Ref. [4] for $R_{\rm e} = 7000$ are well fitted by the $6^{\rm th}$ order polynomial. All the constants do not vary significantly with $R_{\rm e}$. Interesting as well, there is little difference between the results related with Refs. [3] and [4]. Since the nozzle configurations and the boundary

conditions in Refs. [3] and [4] are quite different, we can conclude that constants B_1, B_2 and thus C_1–C_4 are all weakly correlated with the Reynolds number. As demonstrated on the plot, we approximately obtain that $C_1 = 0.6$, $C_2 = 0.66$, $C_3 = 1.34$ and $C_4 = 1.28$.

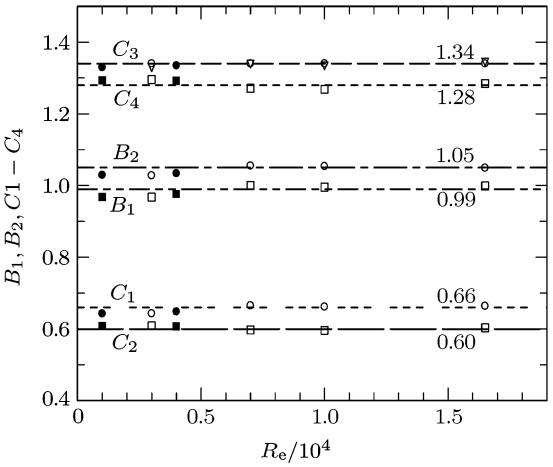


Fig. 4. Values of B_1, B_2, and $C_1 - C_4$ for different profiles of $e(\xi)$. Open symbols are results from Ref. [4]; closed symbols are results from Ref. [3].

3.2. Mean velocity field

Figure 5 presents lateral distributions of $f = \langle U\rangle/U_c$ obtained at $x/H \approx 50$ in the self-similar region by Deo *et al.*[4] and Namar *et al.*[3] for several Reynolds numbers. As expected, when plotting $f = \langle U\rangle/U_c$ against $\eta = y/y_{1/2}$ all the data points collapse well no matter how different the Reynolds numbers and other initial conditions are. This implies that f is independent of initial conditions. Figure 5 also demonstrates that f can be well approximated by the Gaussian distribution $f(\eta) = \mathrm{e}^{-\eta^2 \ln 2}$.

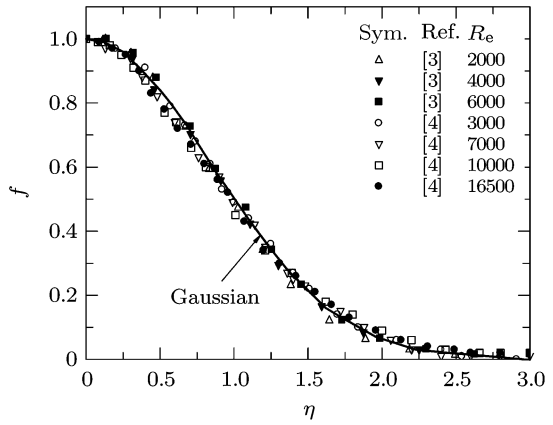


Fig. 5. Lateral distributions of $\langle U\rangle/U_c$ in the self-similar region.

Figures 6(a) and 7(a) show, respectively, the half-width of the mean velocity field and the centreline mean velocity decay obtained by Namar *et al.*[3] and Deo *et al.*[4] Apparently, equations (16) and (17) are well satisfied by almost all data for $x/H \geq 10$, suggesting the establishment of the self-similarity of the mean velocity field. Figures 6(b) and 7(b) demonstrate that as R_e increases, both K_1 and K_2 decrease.

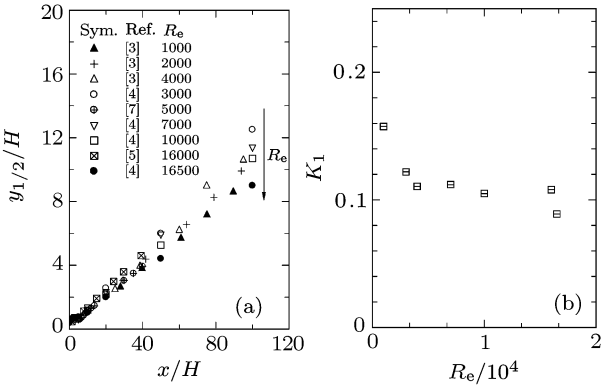


Fig. 6. (a) Dependence of the half width of the mean velocity field on Reynolds number. (b) Dependence of K_1 on Reyonlds number.

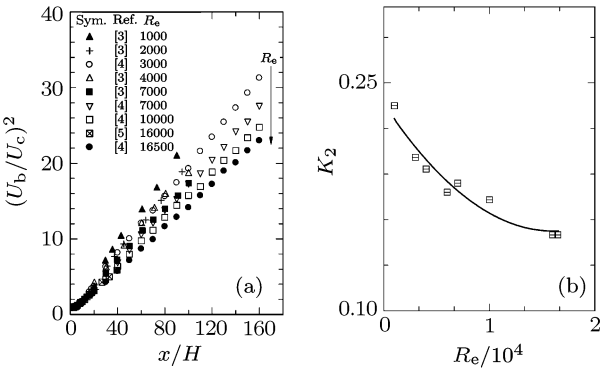


Fig. 7. (a) Inverse variation of the centreline mean velocity. (b) Dependence of K_2 on Reyonlds number.

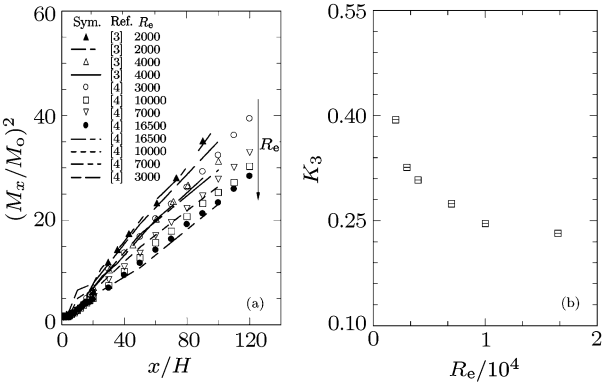


Fig. 8. (a) Entrainment rates of plane jets obtained from direct measurements (curves) and from indirect measurements based on Eq. (10) (dots). (b) Dependence of K_3 on Reyonlds number.

Figure 8(a) shows direct and indirect measurements of the entrainment rates (M_x/M_o) of the turbulent plane jets at various Reynolds numbers. Note that the direct measurement data were obtained from the integration of the lateral profiles of the mean velocity, while those indirect data were estimated based on Eq. (1) and C_4 (based on the centreline velocity ratio U_c/U_b). Quite obviously, the direct and the indirect results agree very well, thus validating Eq. (1) implicitly. Figure 8(b) demonstrates that the jet with smaller R_e has higher entrainment rate K_3, which may be due to the more organized underlying large-scale structures.

Table 1. Comparison of K_1, K_2 and K_3 obtained from different experiments.[3,4]

R_e	3000[4]	7000[4]	10000[4]	16500[4]	1000[3]	2000[3]	4000[3]
K_1	0.1220	0.1120	0.1050	0.0890	0.1576	0.120	0.1106
K_2	0.2010	0.1840	0.1730	0.150	0.2350	0.202	0.1933
K_3	0.3260	0.2740	0.2460	0.2320		0.3940	0.3080

The experimental data of K_1–K_3 obtained from Figs. 6–8 are plotted in Fig. 9. Also shown on the plot is the ratio K_1/K_2. It is deduced from Eqs. (16) and (17) that $C_2 = K_1/K_2$ and thus $K_1 = C_2K_2$. Obviously, based on the data from Refs. [3] and [4], the direct measurement results of $C_2 = K_1/K_2$ agree very well with that calculated from $C_2 \approx 0.6643B_1B_2^{-2} \approx 0.6$ (see Fig. 4). In other words, once K_2 has been measured, K_1 can be well estimated as $K_1 \approx 0.6K_2$. Similarly, K_3 can be obtained approximately as $K_3 = C_4^2K_2$, where $C_4 \approx 1.4142B_1B_2^{-2}$. Indeed, the analytical and the directly measured results are consistent with each other as displayed on the plot.

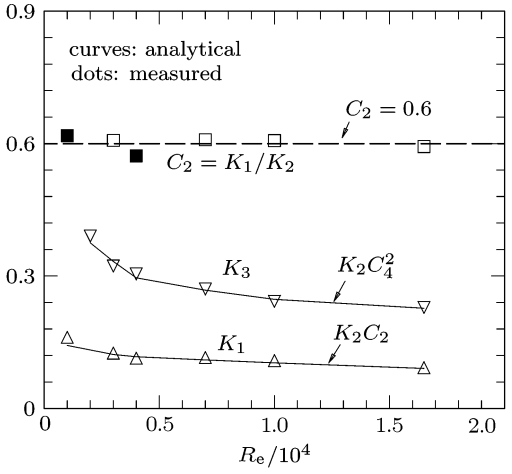


Fig. 9. Analytical and experimental results of C_2, K_1–K_3: closed symbols from Ref. [3]; open symbols from Ref. [4].

3.3. Reynolds stresses

Figures 10 and 11 show, respectively, lateral profiles of the normalized Reynolds normal stresses $g_{11} = \langle u^2\rangle(x,\eta)/U_c^2$, $g_{22} = \langle v^2\rangle(x,\eta)/U_c^2$ and the normalized Reynolds shear stress $g_{12} = \langle uv\rangle/U_c^2$ obtained in the far-field region ($x > 25H$) by the previous investigations.[3–5,7,10,14] Unfortunately, the previous stress data obtained by hot-wire measurements are very scattering! The cause of this scattering is manyfold, e.g., different initial and boundary conditions and experimental errors. We believe the main cause is the uncertainties of the hot-wire measurements.

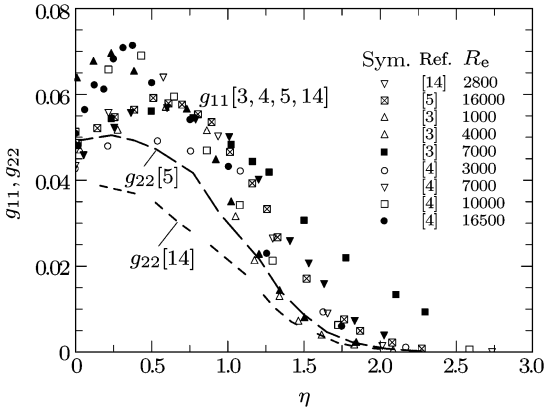


Fig. 10. Lateral profiles of the turbulence intensity components g_{11}, g_{22} in plane jets.

Despite the problem, it can be deduced from Fig. 10 that, in general, g_{11} is significantly larger than g_{22}. To validate Eq. (21) through the experimental results, we estimate g_{12} by taking $K_1 = 0.11$ from Refs. [5] and [14], 0.10 from Refs. [7] and [10]. The results are presented in Fig. 11. Evidently, the prediction of Eq. (21) for g_{12} with $K_1 = 0.11$ and $K_1 = 0.1$ agrees well with the measurements of Ref. [5] and Ref. [10] at $\eta < 1$. We also observe that the results of Eq. (21) differ appreciably from the measurements of Browne *et al.*[7] and Heskestad[14] for $K_1 = 0.10$ and $K_1 = 0.11$. We attribute this difference to the measurement errors for two reasons. First, the measurements for the mean velocity data shown in Fig. 5 are

much more accurate than that for the Reynolds shear stress (and also normal stresses). Second, Eq. (21) is derived from the self-similar equation (19) and the Gaussian distribution given in Eq. (20), which fits well to the profile of $U(y)/U_c(x)$. Hence, we believe that Eq. (21) is valid for estimating g_{12} or the Reynolds shear stress based on the measured mean velocity field.

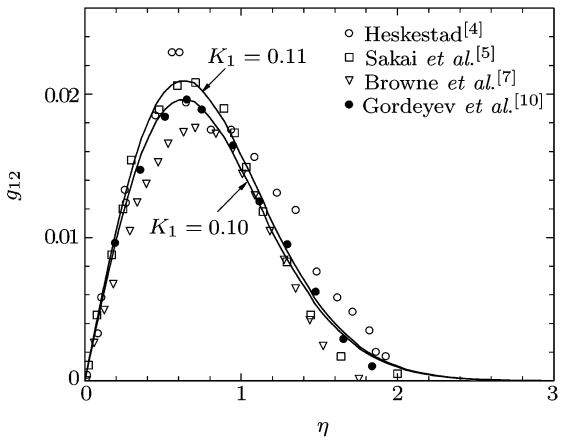


Fig. 11. Lateral normalized profiles of the Reynolds shear stress for $x/H = 40$.

4. Summary

The present study has investigated the effect of initial velocity profiles on the downstream velocity characteristics of a turbulent free plane jet. We have also analysed the velocity-field characteristics of the jet based on the principle of momentum conservation, obtaining several relationships for the jet half-width, the centreline mean velocity, the entrainment rate the Reynolds shear stress and the turbulent viscosity. Some of these relationships have been reported previously, e.g., in Pope,[24] while the last one, equation (21) for self-preservation is given for the first time.

Based on the analytical results and the previous measurements, the following main conclusions can be drawn.

(i) Constants B_1, B_2 in Eqs. (3)–(5) and C_1–C_4 in Eqs. (3), (5), (9), (10) depend very weakly on the exit Reynolds number and perhaps also on other initial conditions. Specifically, their values are estimated to be $C_1 \approx 0.6$, $C_2 \approx 0.66$, $C_3 \approx 1.34$ and $C_4 \approx 1.28$. It follows that the approximations

$$\frac{y_{1/2}}{H} \approx 0.6\left(\frac{U_{oc}}{U_c}\right)^2 \approx 0.66\left(\frac{U_b}{U_c}\right)^2$$

and

$$\frac{M_x}{M_o} \approx 1.34\frac{U_{oc}}{U_c} \approx 1.28\frac{U_b}{U_c}$$

may be generally valid in the flow region downstream from the potential core, which are not subject to the establishment of the self-preservation. These approximations have not been considered so far in the literature.

(ii) The effect of initial mean velocity and RMS velocity profiles on the downstream mean velocity field is embodied in K_1 or K_2 rather than B_1, B_2 and C_1–C_4.

(iii) The jet spread rate K_1 and the entrainment rate K_3 (and thus K_2) may be well estimated from the measurement of the centreline velocity, i.e., $K_1 \approx 0.6K_2$ and $K_3 \approx C_4^2 K_2$.

(iv) The newly-derived analytical relation given in Eq. (21) works reasonably well to estimate the Reynolds shear stress.

References

[1] Mi J, Nobes D S and Nathan G J 2001 *J. Fluid Mech.* **432** 91
[2] George W K 1989 *Advances in Turbulence* **4** 39
[3] Namar I and Ötügen M V 1988 *Exp. Fluids* **6** 387
[4] Deo R C, Mi J and Nathan G J 2008 *Phys. Fluids* **20** 51
[5] Sakai Y, Tanaka N, Yamamoto M and Kushida T 2006 *JSME Int. J. B-Fluid T.* **49** 115
[6] Tanaka N, Sakai Y, Yamamoto M and Kubo T 2006 *JSME Int. J. B-Fluid T.* **49** 899
[7] Browne L W B, Antonia R A, Rajagopalan S and Chambers A J 1982 *IUTAM Symposium* **5** 411
[8] Klein M, Sadiki A and Janicka J 2003 *Int. J. Heat and Fluid Flow* **24** 785
[9] Deo R C, Mi J and Nathan G J 2006 *Exp. Therm. Fluid Sci.* **31** 825
[10] Gordeyev S V and Thomas F O 2000 *J. Fluid Mech.* **414** 145
[11] Deo R C, Mi J and Nathan G J 2007 *Exp. Therm. Fluid Sci.* **32** 545
[12] Deo R C, Mi J and Nathan G J 2007 *Exp. Therm. Fluid Sci.* **32** 596
[13] Mi J, Deo R C and Nathan G J 2005 *Phys. Fluids* **17** 068102
[14] Heskestad G 1965 *J. Appl. Mech.* **32** 721
[15] Thomas F O and Goldschmidt V W 1986 *J. Fluid Mech.* **163** 227
[16] Mi J, Feng B, Deo R C and Nathan G J 2009 *Acta Phy. Sin.* **53** 220 (in Chinese)
[17] Everitt K W and Robbins A G 1973 *J. Fluid Mech.* **88** 563
[18] Sato H 1960 *J. Fluid Mech.* **7** 53
[19] Goldschmidt V W and Bradshaw P 1973 *Phys. Fluids* **16** 354
[20] Thomas F O and Goldschmidt V W 1986 *J. Fluid Mech.* **163** 227
[21] Bradbury L J S 1965 *J. Fluid Mech.* **23** 31
[22] Gutmark E and Wygnanski I 1976 *J. Fluid Mech.* **73** 465
[23] Townsend A A 1976 *The Structure of Turbulent Shear Flow* (Cambridge: Cambridge University Press) p. 126
[24] Pope S B 2000 *Turbulent Flows* (Cambridge: Cambridge University Press) p. 134